Tuijin Jishu/Journal of Propulsion Technology
ISSN: 1001-4055
Vol. 46 No. 3 (2025)

Thermo-Exergic Performance evaluation of Herringbone Finned Absorber Solar Air Heater

[a,c]Rajesh Kumar, [b,c]Sonu Kumar

[a]Department of Mechanical Engineering, Government Engineering College Nawada, Bihar-805111
[b]Department of Mechanical Engineering, Government Engineering College Jehanabad, Bihar-804407
[c]Science, Technology and Technical Education Department, Patna, Bihar

Abstract: This study evaluates the thermal and exergetic performance of a solar air heater with a herringbone finned absorber. Energy and exergy balance equations were formulated and solved iteratively in MATLAB to determine temperature fields and performance metrics under varying mass flow rate, fin pitch, and solar insolation. Herringbone fins enhanced heat transfer by increasing surface area and inducing swirl flow, resulting in higher thermal efficiency than a smooth absorber. Thermal efficiency increased monotonically with mass flow rate, reaching 77.4% at a mass flow rate of 0.41 kg/s for a 1 cm fin pitch. In contrast, exergy efficiency peaked at 5.23% at a flow rate of 0.002 kg/s before declining due to pumping losses. It also rose with insolation, from 1.7% at 400 W/m² to 4.0% at 1000 W/m². The study highlights the trade-off between thermal and exergy performance, offering guidelines for the optimal design of solar air heaters.

Keywords: *Herringbone fins, exergy efficiency, solar air heater.*

1. Introduction

A solar air heater is a widely used device for harnessing solar energy in applications such as crop drying, timber seasoning, space heating, and laundry processes [1]. Despite its versatility, the relatively low thermal efficiency of solar air heaters has been a persistent concern among researchers. To address this limitation, several design modifications have been investigated, including the incorporation of extended surfaces [2,3], corrugated absorber plates [4], artificially roughened surfaces [5,6], and packed bed configurations [7]. Traditionally, the performance of thermal systems has been evaluated using energy analysis. However, this approach does not account for thermodynamic irreversibilities and, therefore, is insufficient for a comprehensive assessment. Exergy analysis, which is grounded in the second law of thermodynamics, overcomes this limitation by quantifying irreversibilities, determining their relative magnitudes, and locating their sources within the system. Consequently, it has become an important tool in the design, optimization, and performance evaluation of thermal systems [8]. Extensive investigations have been carried out on the energy and exergy characteristics of solar air heaters. Hedayatizadeh et al. [9] conducted an exergy-loss-based optimization of a double-pass V-corrugated plate solar air heater, considering corrugation height, glazing spacing, mass flow rate, and collector area as decision variables. Their analysis reported a maximum exergy efficiency of 6.27% at a mass flow rate of 0.005 kg/s, corrugation height of 0.0122 m, glazing distance of 0.0023 m, and collector area of 1.79 m². Esen [10] experimentally examined the thermodynamic performance of a double-flow solar air heater equipped with absorber plate obstacles, and demonstrated that obstacle geometry, orientation, and arrangement substantially improved collector efficiency. Ajam et al. [11] performed exergetic optimization of solar collectors by incorporating variable thermal loss and convective heat transfer coefficients, revealing that optical efficiency had a dominant effect on exergy performance, whereas pipe diameter exerted only a minor influence. They further observed that exergy efficiency increased with insolation and inlet temperature until reaching an optimum threshold, beyond which it declined. Bahrehmand et al. [12] proposed an analytical model to evaluate single- and double-glass solar air heaters with fins, both with and without metal sheet attachments, under forced convection. The results showed that the fin–metal sheet configuration achieved the best performance, while the double-glass design with metal sheets produced negative exergy efficiencies at Reynolds numbers exceeding 22,000. Benli [13] conducted analytical and experimental comparisons of five collector geometries (corrugated trapeze, reverse corrugated, reverse trapeze, and flat plate), reporting an inverse relationship between exergy rate, heat transfer, and pressure drop. Similarly, Kurtbas and Drumus [14] tested five absorber plate geometries (0.9 x 0.4 m) and found that higher mass flow rates and appropriately modified surface geometries enhanced system efficiency, with air temperature rise and pressure drop identified as critical factors governing exergy losses. Fin design has also been extensively investigated as a means of enhancing heat transfer. Wavy, zigzag, and herringbone fins have been shown to increase flow path length, generate streamwise and spanwise vortices, and thereby improve fluid mixing and thermal transport [15,16]. The earliest systematic evaluation of herringbone fins was carried out by Beecher and Fagan [17], who examined 21 different configurations and proposed Nusselt number correlations. Subsequent work by Goldstein and Sparrow [16] demonstrated that herringbone fins could yield up to 45% higher mass transfer rates compared to conventional plate fins, albeit with a corresponding increase in pressure drop. More recently, Kumar and Chand [18] applied herringbone fins in solar air heaters and analyzed the effects of corrugation angle (ϕ), fin spacing ratio (Fp/2A), and cross-sectional aspect ratio (Fp/Hf) on Performance.

The present work examines the thermal and exergetic performance of a solar air heater integrated with an absorber surface fitted with herringbone fins. The influence of mass flow rate, fin pitch, and solar radiation intensity is evaluated and benchmarked against a conventional smooth absorber configuration.

2. Thermodynamics analysis:

To comprehensively evaluate the performance of a solar air heater, both the quantitative (energy) and qualitative (exergy) aspects of the thermal processes must be considered.

2.1 Energy Analysis:

Fig.1 illustrates the schematic configuration of the solar air heater incorporating an absorber surface with herringbone fins, along with the associated geometrical parameters and heat transfer coefficients relevant to the heat exchange process.

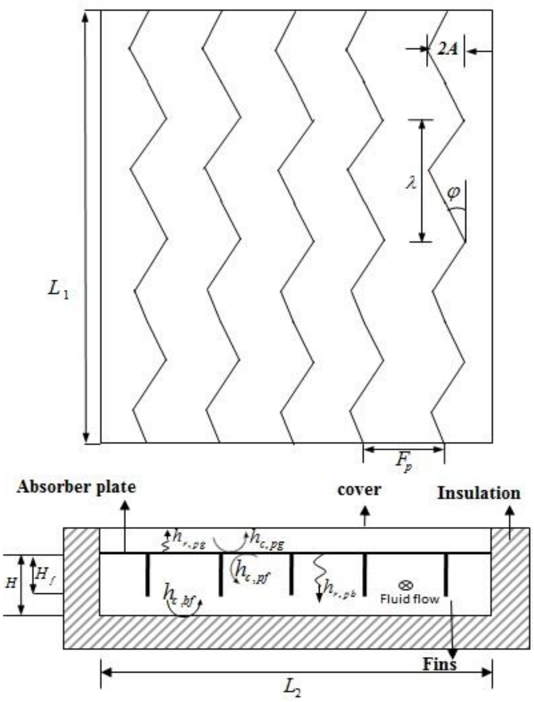

Fig. 1. Schematic diagram (top and front view) of the solar air heater with herringbone fins with their geometrical descriptions.

The first-law (energy) analysis of the system is carried out by formulating energy balance equations for the glass cover, absorber plate, air stream, and bottom plate under the following simplifying assumptions [1]:

(a) The system operates under steady-state conditions.
(b) Air leakage and edge heat losses are neglected.
(c) The temperature drop across the glass cover is assumed to be negligible.
(d) The air temperature is considered to vary only along the flow direction.

Glass cover:

$$\alpha_{gc} I + (h_{r,ap-gc} + h_{c,ap-gc})(T_{ap} - T_{gc}) = (h_w + h_{r,gc-am})(T_{gc} - T_{am}) \tag{1}$$

Absorber plate:

$$I \alpha_{ap} \tau_{gc} = (h_{r,ap-gc} + h_{c,ap-gc})(T_{ap} - T_{gc}) + h_{r,ap-bo}(T_{ap} - T_{bo}) + h_{c,ap-f}(T_{ap} - T_f) + (NA_3 / A_{ap})(T_{ap} - T_f) \tag{2}$$

Bottom plate:

$$h_{r,ap-bo}(T_{ap} - T_{bo}) + h_{c,f-bo}(T_f - T_{bo}) = U_b(T_{bo} - T_{am}) \tag{3}$$

Air:

$$h_{c,ap-f}(T_{ap} - T_f) + (NA_3 / A_{ap})(T_{ap} - T_f) = 2(\dot{m} c_p / A_{ap})(T_f - T_i) + h_{c,f-bo}(T_f - T_{bo}) \tag{4}$$

where $A_3 = \dfrac{mk_{fn} A_{fn}\left[\sinh A_1 + A_2 \cosh A_1\right]}{\cosh A_1 + A_2 \sinh A_1}$ in which $A_1 = mH_f$ and $A_2 = \dfrac{h_{c,ap-f}}{mk_{fn}}$

2.1.1. Heat transfer coefficients and pressure drop

The heat transfer coefficients associated with Eqs. (1)-(4) are evaluated using the following relations. The convective heat transfer coefficient of air flowing over the glass cover is expressed as [2]:

$$h_w = 2.8 + 3.0 V_w \tag{5}$$

The radiative heat transfer coefficient between the glass cover and ambient air, absorber plate and glass cover, absorber plate and bottom plate can be obtained as:

$$h_{r,gc-am} = \sigma \varepsilon_{gc}(T_{gc}^4 - T_S^4)/(T_{gc} - T_{am}) \tag{6}$$

where T_S is sky temperature and is given by $T_S = 0.0552 T_{am}^{1.5}$ [2].

$$h_{r,ap-gc} = \frac{\sigma(T_{ap}^2 + T_{gc}^2)(T_{ap} + T_{gc})}{1/\varepsilon_{ap} + 1/\varepsilon_{gc} - 1} \tag{7}$$

$$h_{r,ap-bo} = \frac{\sigma(T_{ap}^2 + T_{bo}^2)(T_{ap} + T_{bo})}{1/\varepsilon_{ap} + 1/\varepsilon_{bo} - 1} \tag{8}$$

The free convection heat transfer coefficient for the air between the glass cover and the absorber plate $h_{c,ap-gc}$ can be obtained by the expression:

$$h_{c,ap-gc} = \frac{Nu_{ap-gc}}{L} \tag{9}$$

The corresponding expression for Nu_{ap-gc} can be evaluated using the correlation reported in the literature [1]

$$Nu_{ap-gc} = 1 + 1.44\left[1 - \frac{1708(\sin 1.8\beta)^{1.6}}{Ra\cos\beta}\right]\left[1 - \frac{1708}{Ra\cos\beta}\right]^{+}\left[\left(\frac{Ra\cos\beta}{5803}\right)^{1/3} - 1\right]^{+} \quad (10)$$

where β is the plate tilt angle and the superscript '+' implies that only positive values are considered for the terms in the bracket.

The Rayleigh number Ra can be expressed as:

$$Ra = \frac{g\beta'(T_{ap} - T_{gc})L^3}{\nu\alpha} \quad (11)$$

where β' denotes the volumetric coefficients of expansion expressed as:

$\beta' = 1/T$, in which $T = (T_{ap} + T_{gc})/2$ (Kelvin)

The convective heat transfer coefficient of heated air in the conduit can be calculated as

$$h_{c,ap-f} = h_{c,bo-f} = Nu_{ap-bo}k_{air}/D_h \quad (12)$$

where Nu_{ap-bo} is the Nusselt number for the air in the flow channel and D_h is the characteristic dimension used in defining both Nu_{ap-bo} and Re:

$$D_h = \begin{cases} 2HL_2/(H + L_2) & \text{, plane absorber solar air heater} \\ 2(HF_p - t_f H_f)/(F_p + H_f) & \text{, finned absorber solar air heater} \end{cases} \quad (13)$$

The Nusselt number correlations for airflow inside the smooth duct can be obtained from Heaton et al. [3] for laminar flow and from Kay's data [4] for turbulent flow:

$$Nu_{ap-bo} = \begin{cases} 4.4 + \dfrac{0.00398(0.7\,\mathrm{Re}\;D_h/L_1)^{1.66}}{1 + 0.00114(0.7\,\mathrm{Re}\;D_h/L_1)^{1.12}} & \text{laminar flow} \\ 0.00158\,\mathrm{Re}^{0.8} & \text{turbulent flow} \end{cases} \quad (14)$$

For herringbone corrugated channels, the Nusselt number may be expressed in terms of the Colburn factor (j) [5]

$$j = 0.0836\,\mathrm{Re}^{-0.2309}\left(\frac{F_p}{H_f}\right)^{0.1284}\left(\frac{F_p}{2A}\right)^{-0.153}\left(\frac{L_1}{\lambda}\right)^{-0.326} \quad (15)$$

$$Nu_{ap-bo} = j\,\mathrm{Re}\,\mathrm{Pr}^{1/3} \quad (16)$$

The pressure drop across the duct is given by

$$\Delta p = \frac{4f\rho L_1 V^2}{2D_h} \quad (17)$$

where f is the Fanning friction factor, determined as follows:

For flow in the smooth rectangular channel [23]

$$f = \begin{cases} 16/\mathrm{Re} & \text{laminar flow} \\ 0.079\,\mathrm{Re}^{-0.25} & \text{turbulent flow} \end{cases} \quad (18)$$

For flow in the herringbone corrugated channel [5]

$$f = 1.16\,\mathrm{Re}^{-0.309}\left(\frac{F_p}{H_f}\right)^{0.3703}\left(\frac{F_p}{2A}\right)^{-0.25}\left(\frac{L_1}{\lambda}\right)^{-0.1152}$$

2.2. Exergy Analysis:

Exergy analysis has been performed under the following assumptions:

(a) The process is steady-state and steady-flow.

(b) Kinetic and potential energy changes are negligible.
(c) Air behaves as an ideal gas with constant specific heat.
(d) The effect of air humidity is neglected.

By treating the solar air heater as the control volume, the general exergy balance equation under steady-flow conditions can be expressed as:

$$\dot{E}x_i - \dot{E}x_o - \dot{E}x_d = 0 \quad (19)$$

where Ex_i and $\dot{E}x_o$ denoted exergy rate entering and leaving the system, respectively, and Ex_d represents total exergy destruction within the system.

The inlet exergy rate Ex_i comprises the exergy rate associated with the inlet fluid stream as well as the radiated exergy rate from the sun.

$$\dot{E}x_i = \dot{E}x_{i,\mathrm{f}} + \dot{E}x_r \quad (20)$$

The exergy rate ' Ex_i ' associated with inlet fluid flow and radiated exergy rate from the sun can be given by:

$$Ex_{i,f} = \dot{m}c_p\left[(T_i - T_{am}) - T_a \ln(T_i / T_{am})\right] + \dot{m}RT_{am}\ln(P_i / P_{am}) \quad (21)$$

$$Ex_r = \left(1 - T_{am} / T_s\right) IA_c \quad (22)$$

The outlet exergy rate $\dot{E}x_o$ consists of exergy rate carried by outlet fluid stream along with the exergy loss caused by heat leakage to the ambient and is expressed as:

$$\dot{E}x_o = \dot{E}x_{o,f} + \dot{E}x_l \quad (23)$$

$$Ex_{o,f} = \dot{m}c_p\left[(T_o - T_{am}) - T_{am}\ln(T_o / T_{am})\right] + \dot{m}RT_{am}\ln(P_o / P_{am}) \quad (24)$$

$$\dot{E}x_l = U_L A_{ap}\left(T_{ap} - T_{am}\right)\left(1 - T_{am} / T_{ap}\right) \quad (25)$$

where U_L is overall loss coefficient, calculated as:

$$U_L = U_b + U_t \quad (26)$$

In which U_t is top loss coefficient, given by the relation

$$U_t = \left(\frac{1}{h_{r,ap-gc} + h_{c,ap-gc}} + \frac{1}{h_{r,gc-am} + h_w}\right)^{-1} \quad (27)$$

The difference between exergy leaving and entering the system is termed as an increase in flow exergy or exergy recovered.

$$\begin{aligned}\dot{E}x_{rec} &= \dot{E}x_{o,f} - \dot{E}x_{i,f} \\ &= \dot{m}c_p\left(T_o - T_i\right) - \dot{m}c_p T_{am}\ln\left(T_o / T_i\right) + \dot{m}RT_{am}\ln\left(P_o / P_i\right)\end{aligned} \quad (28)$$

The second law (exergy) efficiency of a solar air heater system is defined as [8]

$$\eta_{II} = \frac{Exergy\ recovered}{Exergy\ supplied} = \frac{\dot{m}c_p\left(T_o - T_i\right) - \dot{m}c_p T_{am}\ln\left(T_o / T_i\right) + \dot{m}RT_{am}\ln\left(P_o / P_i\right)}{\left(1 - T_{am} / T_s\right) IA_c} \quad (29)$$

where T_s is the apparent temperature of the sun typically taken as 4330 K [9].

3. Numerical calculations and Solution procedure:

To assess the thermal and exergetic performance of the system, it is necessary to determine the temperatures T_{gc}, T_{ap}, T_{bo}, and T_f and the associated heat transfer coefficients. Since many of these coefficients are interdependent on temperature values, obtaining a direct analytical solution becomes challenging. Therefore, an iterative solution procedure is adopted to evaluate the required parameters. For this purpose, computational codes were developed in MATLAB-14, utilizing the system and design parameters summarized in Table 1, unless otherwise specified.

Table 1. Design and operating parameters of solar air heater.

L_1 = 1.2 m	F_p =1cm,2.5cm, 4cm and 5cm	V_w =2.5 m/s	$\dot{m}$ = 0.001-0.06 kg/s	ε_{gc} =0.9
L_2 = 0.4 m	H_f = 0.028m	I=900 W/m^2	k_{ins} = 0.05 W/mK	τ_{gc} =0.88
H = 0.03 m	t_{ins} =0.006 m	T_{am} =300K	k_{fn} =50 W/mK	ε_{ap} =0.95
L = 0.04 m	t_f = 0.001 m	T_i =303K	α_{gc} =0.11	ε_{bc} =0.95
λ = 7cm	A=1.5cm	θ =0°	α_{ap} =0.96	

The calculation procedure was carried out in the following steps:

(i). Initial estimates of the mean temperature of the glass cover, absorber plate, fluid, and the bottom plate were assumed as $[T_{ini}] = [T_{gc}, T_{ap}, T_f, T_{bo}]$.

(ii). Based on these assumed temperatures, the corresponding heat transfer coefficients were evaluated using Eqs. (7)- (18).

(iii). The updated values of the temperatures T_{gc}, T_{ap}, T_f and T_{bo} were calculated.

(iv). The convergence criterion was applied by comparing the updated temperatures $[T_{new}]$ with their previously assumed values $[T_{ini}]$. If the absolute difference exceeded 0.001, the iteration was repeated with the updated temperatures. This process continued until the absolute difference between successive iterations was less than or equal to 0.001.

(v). The final converged values of the mean temperatures and heat transfer coefficients were employed to determine the thermal and exergetic efficiencies of the system.

4. Results and discussion

This section presents the thermal and exergetic performance analysis of the solar air heater equipped with a herringbone-finned absorber. The performance curves are plotted by varying the mass flow rate, fin pitch, and solar insolation.

Fig 2. depicts the variation of thermal efficiency (η_{th}) and exergy (η_{II}) efficiency as a function of mass flow rate for a fin pitch of F_p = 2.5 cm and solar insolation of I=900 W/m^2. As shown, thermal efficiency exhibits a monotonic increase with mass flow rate, primarily due to the enhanced convective heat transfer from the absorber plate to the air at higher flow rates. In contrast, the exergy efficiency initially increases, reaches a maximum at relatively low mass flow rates, and subsequently decreases with further increase in flow rate. This trend is attributed to the increased exergy losses associated with higher mass flow rates, particularly from the absorber plate.

Fig 3. illustrates the variation of thermal efficiency (η_{th}) with mass flow rate for different fin pitches. It is observed that, for all fin pitches, thermal efficiency increases consistently with mass flow rate. Furthermore, the efficiency of the finned configurations remains higher than that of the smooth absorber solar air heater across the entire studied range of mass flow rates. This enhancement is attributed to the incorporation of herringbone fins, which increase the effective heat transfer area, extend the flow path length, and induce vortex formation, thereby improving fluid mixing and enhancing convective heat transfer. Among the examined cases, the smallest fin pitch F_p = 1 cm yields the highest thermal efficiency.

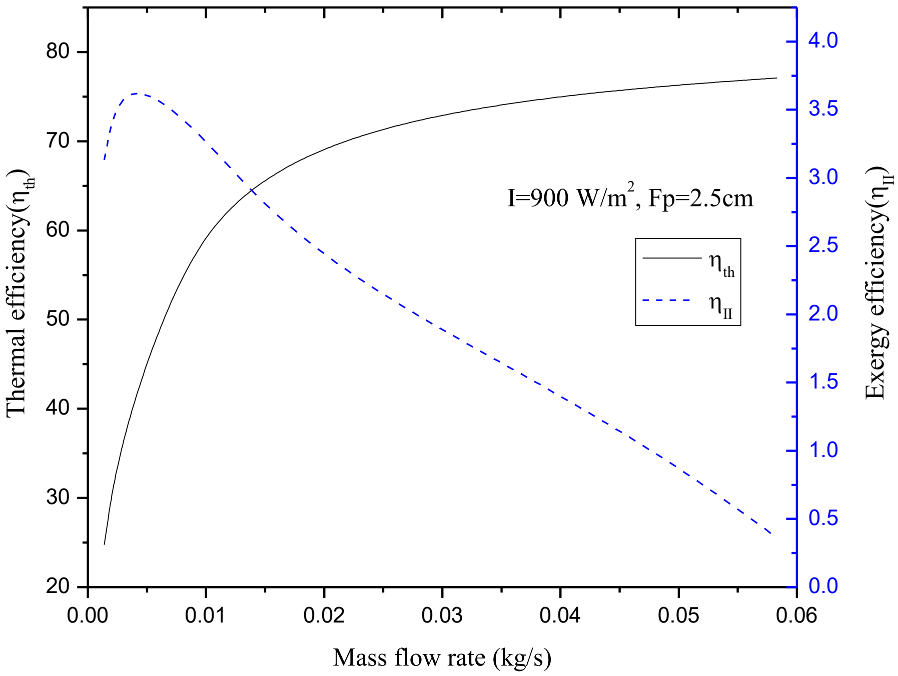

Fig. 2. Variation of thermal and exergy efficiency with mass flow rate for solar air heater with fins.

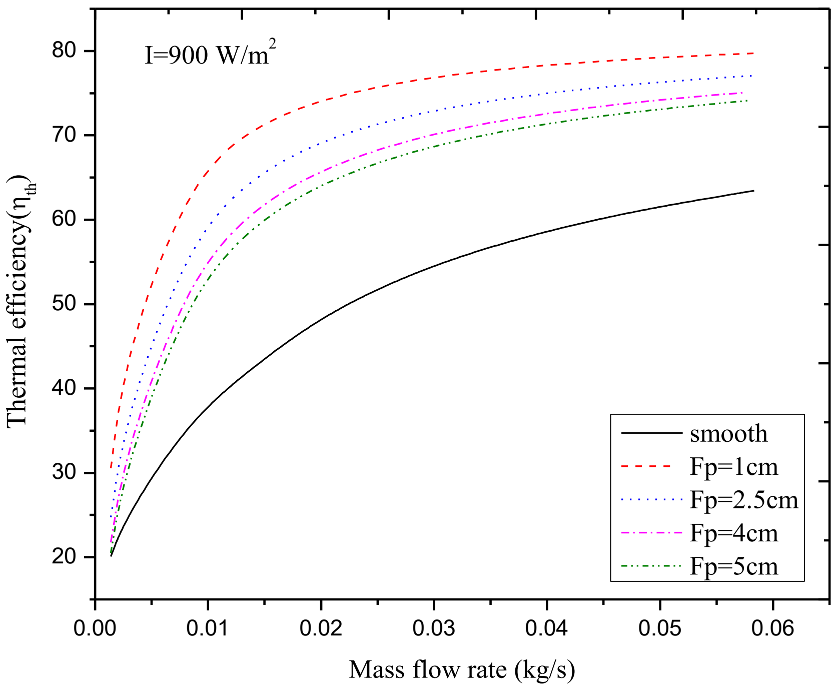

Fig. 3. Variation of thermal efficiency as a function of mass flow rate for various fin pitches.

The behaviour of exergy efficiency (η_{II}) against the mass flow rate for various fin pitches F_p = 1cm, 2.5 cm, 4 cm, and 5 cm is shown in Fig. 4. For all fin configurations, the exergy efficiency initially increases with mass flow rate, reaches a peak value, and then decreases with further increase in flow rate. Up to a mass flow rate of 0.03 kg/s, exergy efficiency improves as the fin pitch decreases; however, beyond this point, the trend reverses, with larger fin pitches exhibiting higher exergy efficiency. This behaviour is attributed to the increased pumping power and associated exergy losses at higher mass flow rates. Consequently, at sufficiently high flow rates, they η_{II} may even attain negative values, as illustrated in Fig. 4.

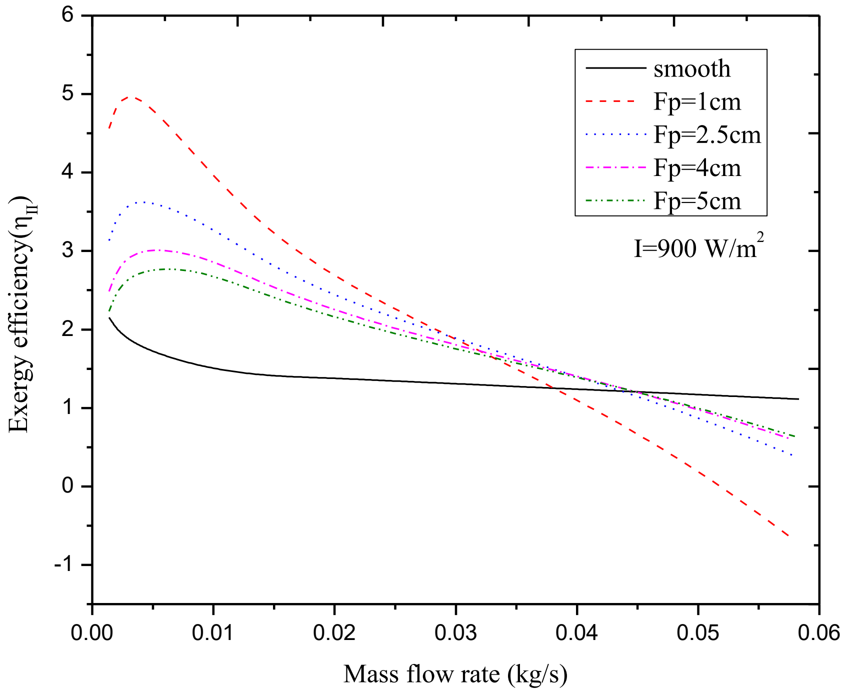

Fig. 4. Variation of exergy efficiency against the mass flow rate and fin pitch.

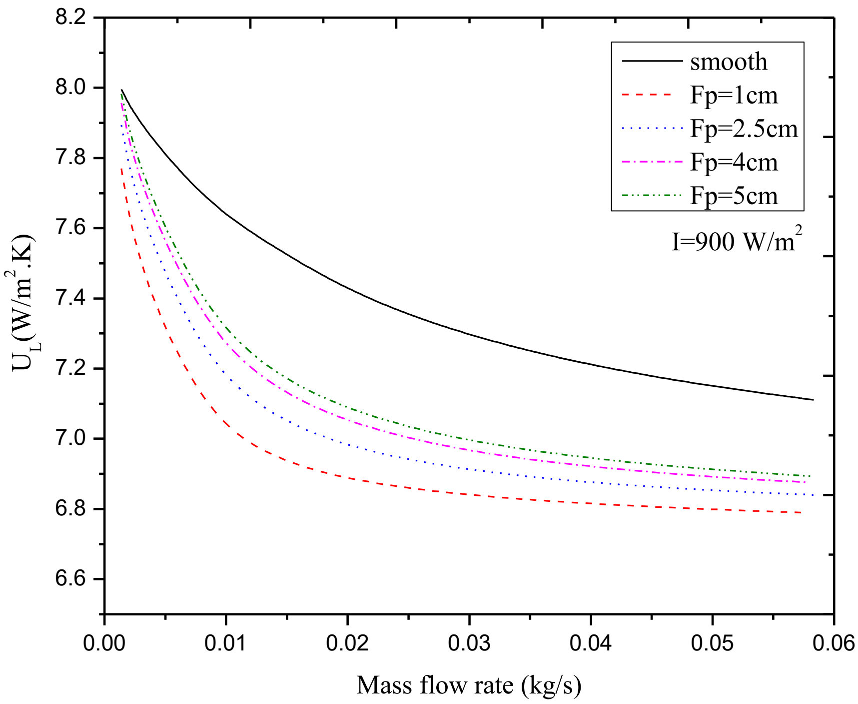

Fig.5. Overall loss coefficient versus mass flow rate for various fin pitches.

Fig.5 illustrates the variation of the overall loss coefficient (U_L) with mass flow rate for different fin pitches. It is observed that (U_L) decreases with increasing mass flow rate for both finned and smooth absorber configurations. However, the overall loss coefficient of the smooth absorber solar air heater is consistently higher than that of the finned configurations. The incorporation of herringbone fins beneath the absorber plate significantly reduces the overall heat losses. For a fixed mass flow rate, increasing the fin pitch results in a higher overall loss coefficient, indicating greater energy dissipation from the absorber plate to the surroundings. For instance, at a mass flow rate of 0.02 kg/s, the addition of herringbone fins with a pitch of 1 cm reduces the overall loss coefficient of the smooth absorber design from 7.5 W/m²K to 6.75 W/m²K.

Figure 6 portrays the influence of mass flow rate and fin pitch on the exergy leakage rate (Ex_l) arising from heat losses from the absorber plate to the ambient. Since exergy leakage rate (Ex_l) depends primarily on the overall loss coefficient 'U_L' and the mean absorber plate temperature 'T_p', a reduction in either parameter leads to a decrease in exergy leakage. With increasing mass flow rate, the mean absorber plate temperature decreases, while a reduction in fin pitch lowers the overall loss coefficient. Consequently, the exergy leakage rate increases with increasing mass flow rate and with decreasing fin pitch, as shown in Fig.6.

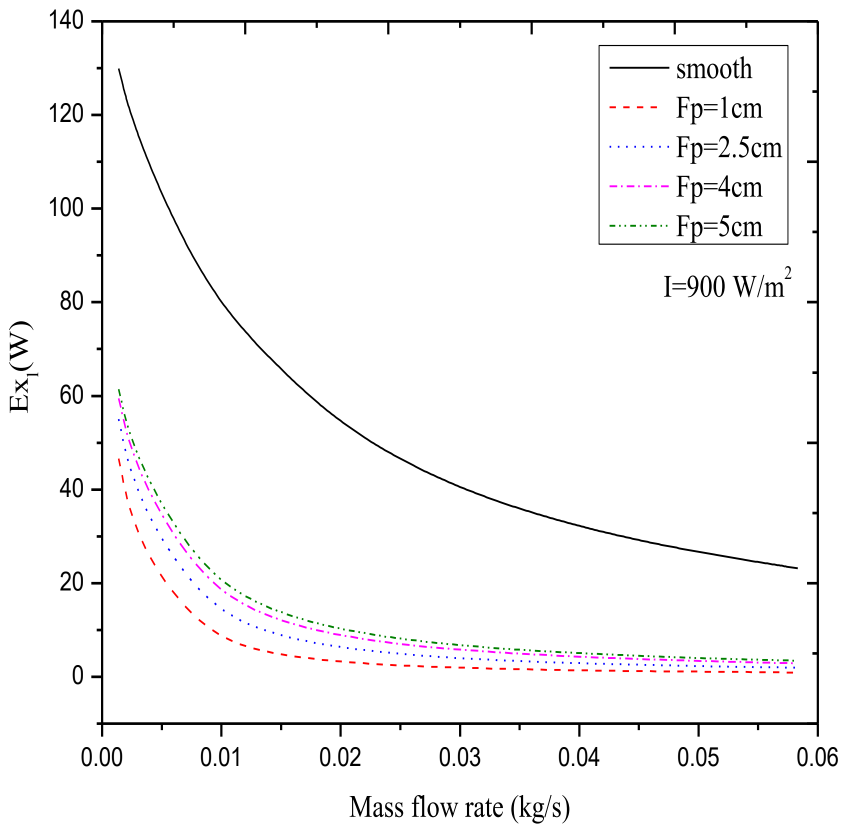

Fig.6. Effect of mass flow rate and fin pitch on the exergy leakage rate.

The response of variation the exergy efficiency (η_{II}) with incident solar radiation 'I' for different fin pitches at a mass flow rate of 0.011kg/s are shown in Fig. 7. It is observed that the exergy efficiency increases with increasing solar radiation intensity and with decreasing fin pitch. As solar radiation rises, the outlet air temperature and consequently the recovered exergy increase. Although the radiative exergy input from the sun also increases, the rate of increase in recovered exergy is greater than that of the supplied exergy, leading to a net improvement in exergy efficiency. For instance, at a fin pitch of 1 cm, exergy efficiency increases from 1.7% to 4.0% as the solar insolation rises from 400 W/m² to 1000 W/m².

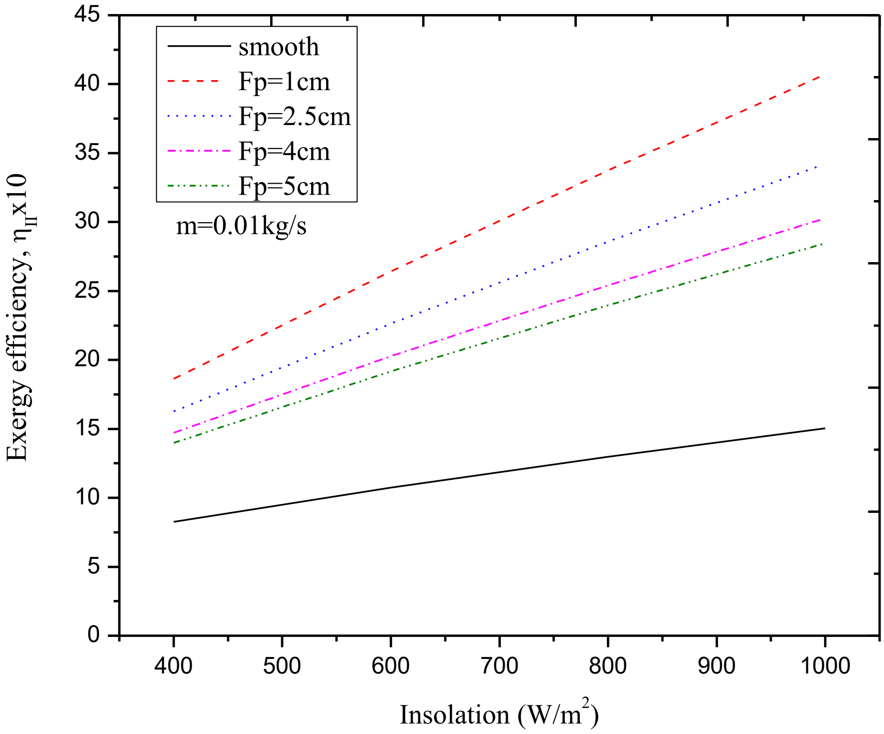

Fig.7. Variation of the exergy efficiency against the solar intensity and fin pitch.

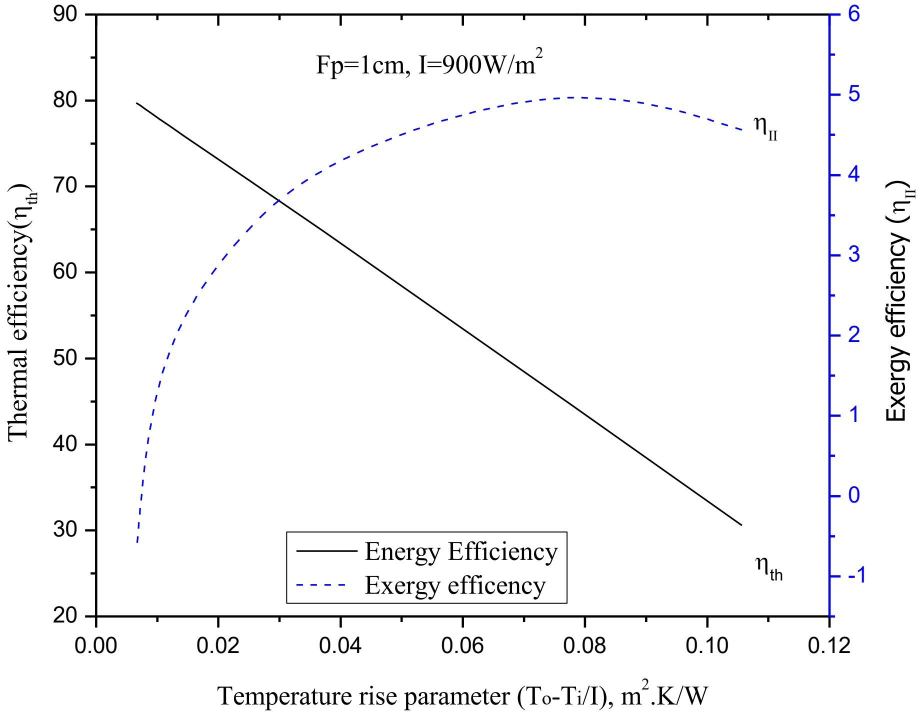

Fig. 8. Thermal and exergetic performance curve as a function of temperature rise parameter ($\Delta T / I$) for fin pitch F_p =1cm and I=900 W/m2

The variation of thermal and exergetic performance curves as function of temperature rise parameter ‘ $\Delta T / I$ ’ for the solar air heater having absorber plate attached with the herringbone fins of fin pitch 1cm for insolation I=900

W/m2 are presented in Fig. 8. The results indicate that thermal efficiency decreases linearly with increasing temperature rise parameter, whereas exergy efficiency increases and approaches an asymptotic value at higher $\Delta T / I$ value.

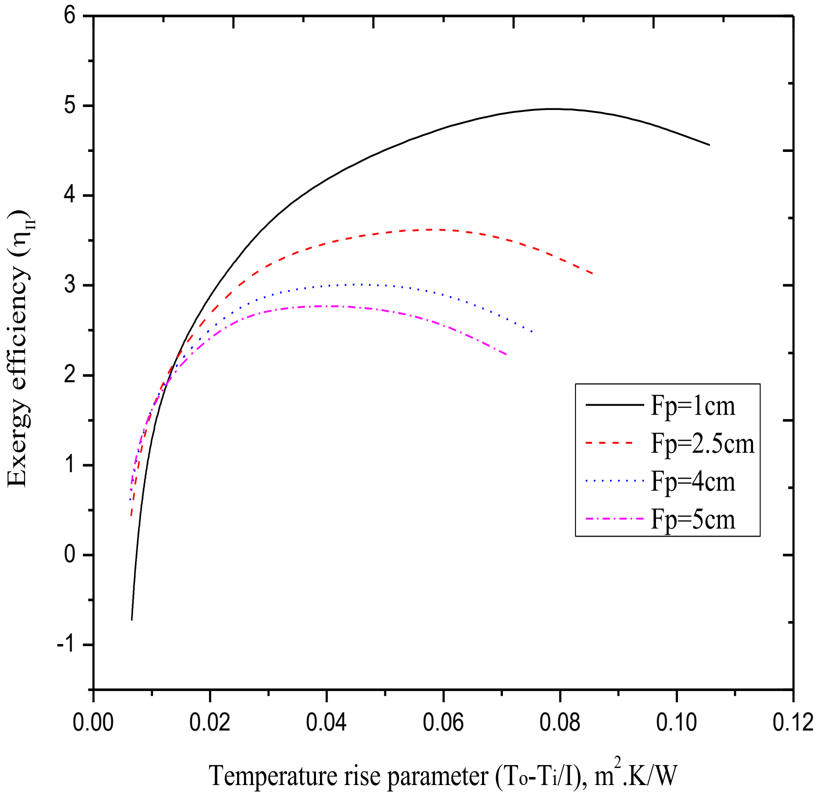

Fig. 9. Exergy efficiency as a function of temperature rise parameter ($\Delta T / I$) and fin pitch.

The plots of exergy efficiency as a function of temperature rise parameter ($\Delta T / I$) and fin pitch are presented in Fig. 9. For all configurations, exergy efficiency increases with an increase in $\Delta T / I$. At lower values of the temperature rise parameter ($\Delta T / I < 0.018$ W/m2K), larger fin pitch yields higher exergy efficiencies. However, beyond this threshold, the trend reverses, and smaller fin pitches result in superior exergy performance.

5. Conclusions

In this study, the thermal and exergetic performance of a solar air heater with an absorber surface integrated with herringbone fins has been analyzed. The effects of mass flow rate, fin pitch, and solar insolation were systematically investigated. The following key conclusions can be drawn:

1. Thermal efficiency is strongly influenced by mass flow rate and fin pitch. The incorporation of herringbone fins with a pitch of 1 cm enhances the thermal efficiency of a smooth absorber solar air heater from 42.5% to 77.4% as the mass flow rate increases from 0.013 to 0.41 kg/s.
2. Thermal and exergy efficiencies exhibit contrasting trends. While thermal efficiency increases monotonically with mass flow rate, exergy efficiency rises to a maximum and subsequently decreases.
3. A reduction in fin pitch improves thermal efficiency across the studied mass flow rate range. However, exergy efficiency increases only up to a mass flow rate of 0.035 kg/s, beyond which the trend reverses.
4. The maximum exergy efficiency of 5.23% is achieved at a mass flow rate of 0.002 kg/s with a fin pitch of 1 cm.
5. At a fin pitch of 1 cm, increasing solar insolation from 400 to 1000 W/m² enhances exergy efficiency from 1.7% to 4.0%.

Nomenclatures:

A_c , A_{ap}	area of collector and absorber plate respectively (m^2)
c_p	specific heat of air (J/kgK)
D_h	hydraulic diameter (m)
$Ex_{i,f}$	exergy at inlet of fluid
$Ex_{o,f}$	exergy at outlet of fluid
$Ex_{r,f}$	exergy radiated from the sun (W)
Ex_l	exergy leakage rate due to heat leakage from the control volume to ambient (W)
F_p	fin pitch (distance between two fins, m)
f	fanning friction factor
H	duct height (m)
H_f	fins height (m)
h_w	heat transfer coefficient due to wind flowing over the glass cover (W/m^2K)
$h_{r,gc-am}$	radiative heat transfer coefficient between glass cover and ambient (W/m^2K)
$h_{r,ap-gc}$	radiative heat transfer coefficient between absorber plate and glass cover (W/m^2K)
$h_{r,ap-bo}$	radiative heat transfer coefficient between absorber plate and bottom plate (W/m^2K)
$h_{c,ap-gc}$	convective heat transfer coefficient between absorber plate and glass cover (W/m2K)
$h_{c,ap-f}$	convective heat transfer coefficient between absorber plate and air stream (W/m^2K)
$h_{c,f-bo}$	convective heat transfer coefficient between fluid and bottom plate (W/m^2K)
I	radiation intensity (W/m^2)
k_{air} , k_{ins} , k_{fn}	thermal conductivity of air , insulation and fins respectively (W/mK)
L	distance between glass cover and absorber plate (m)
L_1	length of the collector (m)
L_2	width of the collector (m)
$\dot{m}$	mass flow rate of air (kg/s)
N	number of fins
Nu_{ap-gc}	Nusselt number between absorber plate and glass cover.
Nu_{ap-bo}	Nusselt number between absorber plate and bottom plate.
Q_u	useful heat gain (W)
Re	Reynolds number
T_i , T_o	inlet and outlet temperature of air (K)
T_{am}	ambient temperature (K)
T_{gc} , T_{ap} , T_{bo} , T_f	average temperature of glass cover, absorber plate , bottom plate and fluid respectively (K)
t_f , t_{ins}	thickness of fins and insulation respectively (m)
U_b	bottom heat loss coefficient (W/m^2K)
V_w	wind velocity (m/s)
Greek Symbols	
α_{ap} , α_{gc}	absorptivity of absorber plate and glass cover respectively

ε_{ap} , ε_{bo} , ε_{gc}	emissivity of absorber plate, bottom plate and glass cover respectively
σ	Stefan's constant (5.67x10^{-8} Wm^{-2}K^{-4})
Δp	pressure drop (N/m^2)
ρ	density of air (kg/m^3)
η_f	fins efficiency
η_{th} η_{II}	thermal and exergy efficiency respectively

References

[1] J.A. Duffie, W.A. Beckman, Solar Engineering of Thermal Processes: Fourth Edition, Fourth, John Wiley & Sons, 2013.
[2] M.F. Pakdaman, A. Lashkari, H.B. Tabrizi, R. Hosseini, Performance evaluation of a natural-convection solar air-heater with a rectangular-finned absorber plate. Energy conversion and management. (2011) 52(2), 1215-1225.
[3] S. Rai, P. Chand, S.P. Sharma, An analytical investigations on thermal and thermohydraulic performance of offset finned absorber solar air heater, Sol. Energy. 153 (2017) 25–40.
[4] A.A. El-Sebaii, S. Aboul-Enein, M.R.I. Ramadan, S.M. Shalaby, B.M. Moharram, Investigation of thermal performance of-double pass-flat and v-corrugated plate solar air heaters, Energy. 36 (2011) 1076–1086.
[5] R.P. Saini, J. Verma, Heat transfer and friction factor correlations for a duct having dimple-shape artificial roughness for solar air heaters, Energy. 33 (2008) 1277–1287.
[6] S. Kumar, R.P. Saini, CFD based performance analysis of a solar air heater duct provided with artificial roughness, Renew. Energy. 34 (2009) 1285–1291.
[7] V.K. Chouksey, S.P. Sharma, Investigations on thermal performance characteristics of wire screen packed bed solar air heater, Sol. Energy. 132 (2016) 591–605.
[8] Y.A. Cengel, M.A. Boles, Thermodyamics an engineering approach, Energy. 1 (2002) 51.
[9] M. Hedayatizadeh, F. Sarhaddi, A. Safavinejad, F. Ranjbar, H. Chaji, Exergy loss-based efficiency optimization of a double-pass/glazed v-corrugated plate solar air heater, Energy. 94 (2016) 799–810.
[10] H. Esen, Experimental energy and exergy analysis of a double-flow solar air heater having different obstacles on absorber plates, Build. Environ. 43 (2008) 1046–1054.
[11] H. Ajam, S. Farahat, F. Sarhaddi, Exergetic optimization of solar air heaters and comparison with energy analysis, Int. J. Thermodyn. 8 (2005) 183–190.
[12] D. Bahrehmand, M. Ameri, M. Gholampour, Energy and exergy analysis of different solar air collector systems with forced convection, Renew. Energy. 83 (2015) 1119–1130.
[13] H. Benli, Experimentally derived efficiency and exergy analysis of a new solar air heater having different surface shapes, Renew. Energy. 50 (2013) 58–67.
[14] İ. Kurtbas, A. Durmuş, Efficiency and exergy analysis of a new solar air heater, Renew. Energy. 29 (2004) 1489–1501.
[15] M.M. Ali, S. Ramadhyani, Experiments on Convective Heat Transfer in Corrugated Channels, Exp. Heat Transf. 5 (1992) 175–193.
[16] J.L. Goldstein, E.M. Sparrow, Experiments on the Transfer Characteristics of a Corrugated Fin and Tube Heat Exchanger Configuration, J. Heat Transfer. 98 (1976) 26–34.
[17] C. Wang, J. Liaw, B. Yang, International Journal of Heat and Mass Transfer Airside performance of herringbone wavy fin-and-tube heat exchangers – data with larger diameter tube, Int. J. Heat Mass Transf. 54 (2011) 1024–1029.
[18] R. Kumar, P. Chand, Performance enhancement of solar air heater using herringbone corrugated fins, Energy. 127 (2017) 271–279.
[19] J.H. Watmuff, W.W.S. Charters, D. Proctor, Solar and wind induced external coefficients - Solar collectors, Coop. Mediterr. Pour l'Energie Solaire, Rev. Int. d'Heliotechnique, 2nd Quarter, 1977, P. 56. (1977) 56.

[20] H.S. Heaton, W.C. Reynolds, W.M. Kays, Heat transfer in annular passages. Simultaneous development of velocity and temperature fields in laminar flow, Int. J. Heat Mass Transf. 7 (1964) 763–781.
[21] W. Kays, M. Crawford, H. Iacovides, F.P. Incropera, D.P. DeWitt, T.L. Bergman, A.S. Lavine, Convective heat and mass transfer, third, 1993.
[22] D. Junqi, C. Jiangping, C. Zhijiu, Z. Yimin, Z. Wenfeng, Heat transfer and pressure drop correlations for the wavy fin and flat tube heat exchangers, Appl. Therm. Eng. 27 (2007) 2066–2073.
[23] M.K. Gupta, S.C. Kaushik, Exergetic performance evaluation and parametric studies of solar air heater, Energy. 33 (2008) 1691–1702.
[24] S.A. Kalogirou, S. Karellas, K. Braimakis, C. Stanciu, V. Badescu, Exergy analysis of solar thermal collectors and processes, Prog. Energy Combust. Sci. 56 (2016) 106–137.
[25] M.K. Gupta, S.C. Kaushik, Performance evaluation of solar air heater for various artificial roughness geometries based on energy, effective and exergy efficiencies, Renew. Energy. 34 (2009) 465–476.